X-ray spectrometer with a low-cost SiC photodiode

Article (Published Version)

Nuclear Inst. and Methods in Physics Research, A 887 (2018) 138–143

Contents lists available at ScienceDirect

Nuclear Inst. and Methods in Physics Research, A

journal homepage: www.elsevier.com/locate/nima

X-ray spectrometer with a low-cost SiC photodiode

S. Zhao *, G. Lioliou, A.M. Barnett

Space Research Group, School of Engineering and Informatics, University of Sussex, Falmer, Brighton BN1 9QT, UK

ARTICLE INFO

Keywords:
X-ray detector
Photodiode
Silicon carbide
COTS
Energy response

ABSTRACT

A low-cost Commercial-Off-The-Shelf (COTS) 4H-SiC 0.06 mm^2 UV p-n photodiode was coupled to a low-noise charge-sensitive preamplifier and used as photon counting X-ray spectrometer. The photodiode/spectrometer was investigated at X-ray energies from 4.95 keV to 21.17 keV: a Mo cathode X-ray tube was used to fluoresce eight high-purity metal foils to produce characteristic X-ray emission lines which were used to characterise the instrument. The energy resolution (full width at half maximum, *FWHM*) of the spectrometer was found to be 1.6 keV to 1.8 keV, across the energy range. The energy linearity of the detector/spectrometer (i.e. the detector's charge output per photon as a function of incident photon energy across the 4.95 keV to 21.17 keV energy range), as well as the count rate linearity of the detector/spectrometer (i.e. number of detected photons as a function of photon fluence at a specific energy) were investigated. The energy linearity of the detector/spectrometer was linear with an error $<\pm$ 0.7 %; the count rate linearity of the detector/spectrometer was linear with an error $<\pm$ 2 %. The use of COTS SiC photodiodes as detectors for X-ray spectrometers is attractive for nanosatellite/CubeSat applications (including solar flare monitoring), and for cost sensitive industrial uses.

1. Introduction

A large number of compound semiconductors have been studied for radiation detection and spectroscopy applications, including GaAs [1–3], AlGaAs [4–6], AlInP [7,8], CdZnTe [9,10], and SiC [11–18]. As one of the wide bandgap (4H-SiC = 3.27 eV [13]) semiconductors, SiC brings the benefits of low leakage currents across a wide range temperatures [14,19,20] and high radiation tolerance [21–24]. Thus, SiC detectors are attractive options for space missions and terrestrial applications that have mass, power, and volume restrictions, since the requirements for cooling and shielding for SiC detectors can be less onerous than for silicon detectors. Within space science and astronomy, SiC detectors may find applicability for in situ and remote X-ray fluorescence (XRF) spectrometry of planetary surfaces in high temperature or intense radiation environments [25–27], as well as for investigation of planetary radiation environments, and near-sun heliophysics and X-ray astrophysics. Terrestrial applications for such detectors include mineral analysis and machine condition monitoring.

Most work on SiC X-ray detectors has concentrated on custom-made devices. However, with the increasing commercial availability of SiC UV photodiodes, interest has been generated in repurposing SiC UV photodiodes as low-cost high temperature tolerant and radiation-hard X-ray detectors. Such use of readily available Commercial-Off-The-Shelf (COTS) technology is of potential value in budget-limited applications such as university-led CubeSat missions.

Previously, results have been reported showing that commercial 4H-SiC p-n photodiodes (manufactured by sglux SolGel Technologies GmbH, Berlin, Germany [28], and purchased from a standard electronics retailer) can be used to spectroscopically detect X-ray photons from an ^{55}Fe radioisotope X-ray source (Mn $K\alpha$ = 5.9 keV; Mn $K\beta$ = 6.49 keV) at room temperature [29] and at temperatures from 100 °C to 0 °C [30]. The geometry of the devices can be found in Ref. [31]. In this paper, we extend the characterisation of this type of photodiode (area = 0.06 mm^2) across the energy range 4.95 keV to 21.17 keV, using eight different high purity metal foils fluoresced by an X-ray tube with a Mo cathode. The photodiode was uncooled throughout the experiment and was maintained at a temperature of 33 °C. The photodiode was supplied mounted in a TO-18 package. In order to directly illuminate the device with X-rays, the UV window of the TO-18 package was removed, as shown in Fig. 1.

2. The photodiode

2.1. Current–voltage characteristics

Previous measurements of the device's current–voltage characteristics showed that its leakage current at temperatures <40 °C was too

* Corresponding author.
E-mail address: Shifan.Zhao@sussex.ac.uk (S. Zhao).

https://doi.org/10.1016/j.nima.2018.01.054
Received 20 September 2017; Received in revised form 12 January 2018; Accepted 15 January 2018

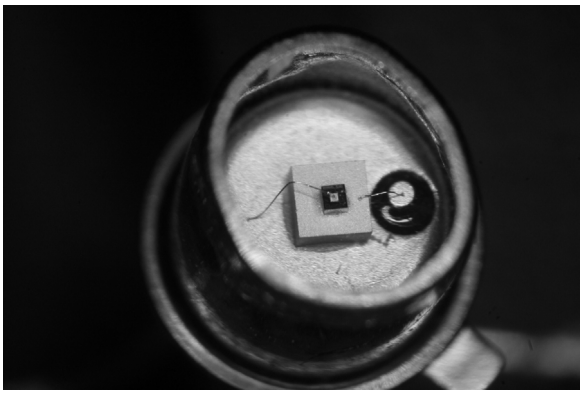

Fig. 1. Photograph of packaged 0.06 mm^2 SiC photodiode with UV window removed.

small to be measured with the available experimental set up, even when the detector was operated at high (100 V) reverse bias [30]. However, because the new X-ray measurements reported in Sections 3.1 and 3.4 of the present article used long accumulation times (14,000 s and 6 h, respectively) with the device kept reverse biased for these periods, measurements were conducted to determine the time stability of the leakage current. Using a Keithley 6487 Picoammeter/Voltage Source, a TAS Micro MT climatic cabinet, and National Instruments Labview software to automate the measurements, the photodiode's leakage current was measured as a function of time when reverse biased at 100 V for 6 h at 33 °C (the temperature at which the X-ray measurements were conducted). The measurements showed that the leakage current remained constant and low (<0.2 pA) throughout the 6 h period.

2.2. Capacitance–voltage characteristics

Measurements of the diode's capacitance as a function of applied reverse bias have been reported at temperatures from 140 °C to 0 °C, in 20 °C steps [30]. However, since the new X-ray characterisation reported in Sections 3.1–3.4 of the present article was conducted at 33 °C (a temperature at which capacitance measurements have not been previously reported for this diode), for completeness, the capacitance of the packaged 0.06 mm^2 SiC photodiode was measured as a function of applied reverse bias at 33 °C. An HP 4275 A Multi Frequency LCR meter was used, in conjunction with a Keithley 6487 Picoammeter/Voltage Source to bias the device, and a TAS Micro MT climatic cabinet for temperature control. The device was installed inside the cabinet and left to stabilise at 33 °C for 30 min before starting the measurement. The AC test voltage signal magnitude and frequency of the LCR meter were set at 60 mV r.m.s. and 1 MHz, respectively. National Instruments Labview software was used to automate the capacitance measurements.

In order to extract the capacitance of the photodiode itself, and separate it from the capacitance of the package (the photodiode and package were considered to be connected in parallel), a sacrificial device of the same type but with its bondwires removed was also measured to yield the packaging capacitance. The capacitance of the photodiode was calculated by subtracting the packaging capacitance (0.75 pF ± 0.01 pF) from the measured total capacitance of the packaged device. The depletion width, W, of the photodiode

$$W = \frac{\epsilon_0 \epsilon_r A}{C} \tag{1}$$

is inversely proportional to the capacitance, C, thus it was calculated using the measured capacitance of the photodiode (Fig. 2a) [32], where ϵ_0 was the permittivity of the vacuum, ϵ_r was the dielectric constant of 4H-SiC 9.7 [33], and A was the diode area. The measured capacitance, the calculated depletion width and the C^{-2} of the photodiode as functions of applied reverse bias at 33 °C are shown in Fig. 2, respectively. The photodiode appeared to be fully depleted at reverse biases ≥ 100 V, with the implied thickness of the depletion width = 2.69 μm ±0.04 μm at 100 V reverse bias.

Whilst a depletion layer thickness of only 2.69 μm suggests that the quantum efficiency of such a detector would be very low at X-ray energies, previous investigation of these devices showed substantially greater photocurrents than would be expected if the active region of the photodiodes was simply limited to the apparent depletion width [29,30]. Previous photocurrent measurements using an ^{55}Fe radioisotope X-ray source to illuminate the detector suggested that the thickness of the active region was 34.5 μm [30]. In addition to the epitaxial layer, part of the substrate was also considered to constitute the active region of the device; the larger than expected photocurrent that was previously measured may be attributed to the collection of the charge carriers generated around the edge of the depletion region [30]. Because the contact of the photodiode has an optical window, and assuming the top layer of the photodiode was active, the quantum detection efficiency, assuming complete collection of the charge created by the X-rays absorbed in the active region, (i.e. active region thicknesses of 2.69 μm and 34.5 μm) was computed using,

$$QE = 1 - e^{\mu t} \tag{2}$$

where μ is the linear attenuation coefficient at the particular X-ray energy, and t is the thickness of the active region [34]; the calculated quantum detection efficiencies of different thickness of the active regions of the diode are presented in Fig. 3 at X-ray energies up to 24 keV.

3. X-ray measurements

3.1. X-ray fluorescence measurements

In order to accumulate X-ray fluorescence spectra for the eight different high-purity (≥ 98.7%) metal foils (the details of which are shown in Table 1), the photodiode was connected to a custom-made low-noise charge-sensitive preamplifier with a 2N4416 Si input JFET (capacitance = 2 pF). The detector and preamplifier were housed in a single light-tight die cast box, with a 4 μm thick Al X-ray window. The detector was well centred in the middle of the window. An ORTEC 572A shaping amplifier and an ORTEC EASYMCA-8k multi-channel analyser (MCA) were connected to the preamplifier. The preamplifier and diode were installed within a LD Didactic GmbH X-ray apparatus (LD Didactic 554 800) with a Mo X-ray tube (LD Didactic 554 861) and a sample stand goniometer (LD Didactic 554 831) which was used to hold each high purity foil in turn. A custom-made aluminium-PTFE collimator (20 mm central open diameter) was used to collimate the X-rays from the X-ray tube. The sample stand goniometer was set at 45° with respect to the collimator. The detector was positioned at 135° with respect to the collimator, with the detector facing towards the focus of the circle of rotation as shown in Ref. [35]. The distance between the centre of the Mo target tube and the collimator was 40 mm ± 3 mm, the length of the collimator was 105.00 mm ± 0.02 mm, the distance between the collimator and the target stand goniometer was 43 mm ± 1 mm, the distance between the target stand goniometer and the spectrometer was 57 mm ± 1 mm, and the solid angle subtended by the detector from the position of the target stand goniometer was 0.015π sr ±0.001π sr. This geometry minimised the detection of X-rays directly from the tube whilst ensuring good detection of the fluorescence X-rays from the foils. The PTFE inner of the collimator ensured complete absorption of any fluorescence X-rays from the aluminium of the collimator. In order to eliminate any influence of humidity effects upon the detector, dry N_2 gas was flowed through the detector-preamplifier assembly throughout the accumulation of the spectra. The preamplifier was powered continuously throughout the accumulation of the spectra of the foils. The photodiode was reverse biased at 100 V to accumulate each spectrum and was only powered off when the high purity fluorescence

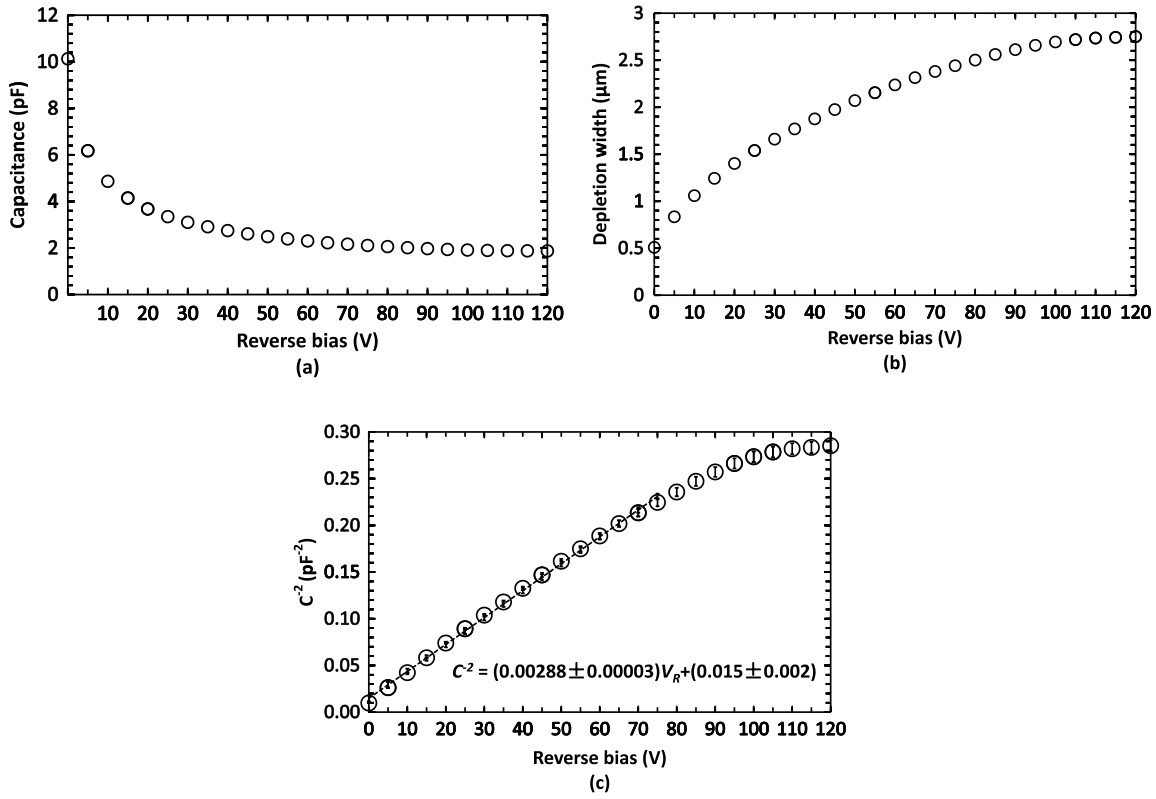

Fig. 2. The measured capacitance, C, (a), calculated apparent depletion width (b), and C^{-2} (c) of the 0.06 mm^2 photodiode as functions of applied reverse bias at 33 °C. The line of best fit was found from 0 V to 75 V as determined by linear least squares fitting is also presented.

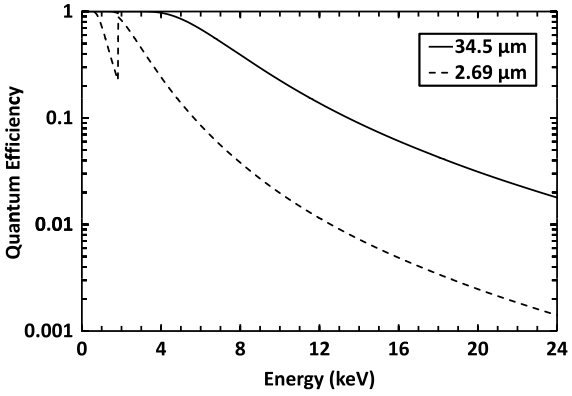

Fig. 3. The calculated quantum detection efficiencies of the 0.06 mm^2 photodiode based on two different thicknesses of active layer (2.69 μm, dashed line; 34.5 μm solid line) as a function of X-ray energy. The discontinuity at 1.8 keV is the Si K absorption edge.

foil was changed. The shaping time of the shaping amplifier was set to the longest available (10 μs) due to the large capacitance and low leakage current of the detector in order to minimise total electronic noise and thus achieve better energy resolution [36,37].

Each foil was fluoresced by X-rays from the Mo X-ray tube, which was operated at a potential difference of 35 kV and a current of 1 mA. X-ray fluorescence spectra were accumulated for each foil using the SiC detector. The accumulation time for each spectrum was 14,000 s. To ensure the temperatures of the detector, preamplifier, and X-ray tube were constant, the X-ray tube was switched on and allowed to warm up for three hours prior to the start of spectrum accumulation in each case; this brought the environment of the detector and preamplifier to a constant temperature of 33 °C [35]. The MCA's charge scale was energy calibrated using the measurement described in Section 3.3; the equation relating photon energy to MCA channel number is given as Eq. (5) in Section 3.3.

Table 1
The high-purity (≥98.7%) metal foils used, together with the energy of the $K\alpha_1$ and $K\beta_1$ X-ray fluorescence lines for each foil. In each case, the primary line used was the $K\alpha_1$ line. The emission line energies were drawn from Ref. [38].

Material	$K\alpha_1$ line energy (keV)	$K\beta_1$ line energy (keV)
V	4.95	5.42
Cr	5.41	5.94
Mn	5.89	6.49
Cu	8.04	8.90
Zn	8.63	9.57
Ge	9.88	10.98
Nb	16.61	18.62
Pd	21.17	23.81

3.2. Spectrometer energy resolution

The "Fano-limited" energy resolution as quantified by the full width at half maximum of a photopeak ($FWHM_{Fano}$) of a non-avalanche photodiode X-ray spectrometer is given by,

$$FWHM_{Fano}\ [\mathrm{eV}] = 2.355\sqrt{FE\omega} \tag{3}$$

where, ω is the average electron–hole pair creation energy (7.8 eV for SiC [12]), F is the Fano factor (0.1 for SiC [14]), and the E is the X-ray photon energy [39].

However, the energy resolution of a photodiode spectrometer is further affected by noise from incomplete charge collection and electronic noise (including parallel white, series white, $1/f$, and dielectric noise) from the detector and preamplifier system, and the shaping amplifier characteristics. Thus the total noise limiting the energy resolution of the spectrometer arises not only from the Fano noise of the detector but

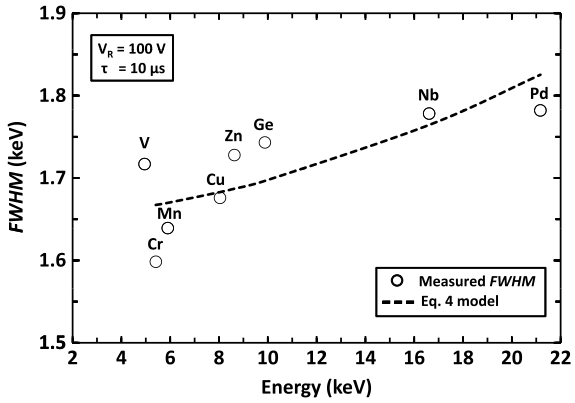

Fig. 4. Measured *FWHM* of the primary X-ray fluorescence lines of eight different materials with the detector operated at 100 V reverse bias (V_R) and using a 10 µs shaping time (τ). The expected *FWHM* from Eq. (4) model is also presented.

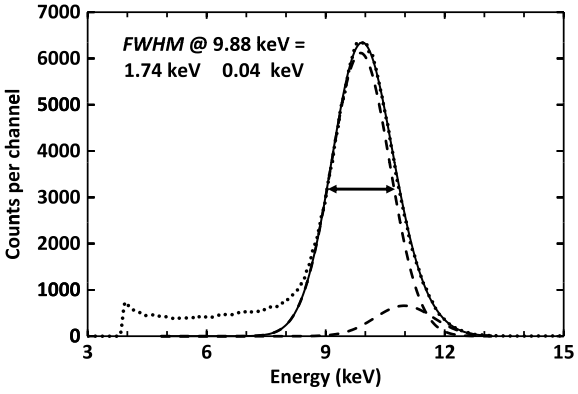

Fig. 5. Ge spectrum accumulated with the SiC photodiode at 100 V reverse bias. The dotted line is the obtained Ge spectrum, the dashed lines are the fitted Ge $K\alpha$ and $K\beta$ peaks, and the solid line is the combination of the fitted Ge $K\alpha$ and $K\beta$ peaks.

also these other sources, such that Eq. (3) becomes,

$$FWHM\ [\mathrm{eV}] = 2.355\sqrt{FE\omega + A^2 + aE^b} \tag{4}$$

where, A is the equivalent noise charge contributions from electronic noise, and aE^b is the incomplete charge collection noise from the detector with a and b being semi-empirical constants determined by best-fitting [39].

A detailed electronic noise analysis for the detector at room temperature was presented in Ref. [29].

For each foil X-ray spectrum obtained, the *FWHM* of the foil's primary X-ray fluorescence line was measured and is shown in Fig. 4. An example X-ray fluorescence spectrum obtained with the Ge ($K\alpha$ = 9.88 keV and $K\beta$ = 10.98 keV [38]) foil is presented in Fig. 5. The expected Fano-limited *FWHM* at 9.88 keV for a SiC detector is 207 eV.

The results in Fig. 4 show that a *FWHM* of 1.6 keV–1.8 keV was achieved across the energy range 4.95 keV–21.17 keV. In each case, the *FWHM* was substantially larger than the expected $FWHM_{Fano}$ due to the influence of the additional noise components in Eq. (4) cf. Eq. (3). At the softest investigated energy V Ka_1 (4.95 keV), the low energy tail of the photopeak was also partly overlapped by the tail of the zero energy noise peak which broadened the apparent *FWHM* of the V $K\alpha$ photopeak.

Excluding V, the measured *FWHM* of the primary fluorescence line of each foil was found to be a function of photon energy. Interestingly, even though the $FWHM_{Fano}$ was calculated to increase with increasing photon energy, the experimentally observed *FWHM* increase could not be explained solely by the increasing Fano noise. The greater than anticipated increase in the measured *FWHM* with increased photon energy may be attributable to incomplete charge collection noise; electronic noise is independent of photon energy but incomplete charge collection noise is energy dependent [40]. As discussed in Section 2.2, it appears that the active region of the photodiode is not restricted to the apparent depletion layer thickness (i.e. the epilayer) but more likely also includes a portion of the device's substrate. Charge transport in high quality 4H-SiC epilayers is such that significant incomplete charge collection is improbable in such an epilayer, especially at the field strengths investigated. However, the same is not necessarily true for the substrate on which the epilayer was grown, particularly because the substrate will have a lower electric field strength within it compared to the epilayer, even when the photodiode is operated at high reverse bias. Given this, it is hypothesised that any apparent incomplete charge collection noise from the detector results from charge carriers created in the substrate as a result of photons absorbed there, rather than from charge carriers created by photons absorbed in the epilayer [30]. Furthermore, generally speaking, lower energy X-ray photons have larger linear attenuation coefficients than higher energy X-ray photons. Thus, given the relative thinness of the detector's epilayer, the energy dependence of the apparent incomplete charge collection noise may have been further enhanced by positional effects: proportionally more photons of higher energy (cf. those of lower energy) will have been absorbed in the possibly lossy substrate compared with the high quality epilayer. Thus, the significance of incomplete charge collection noise from the substrate may have been augmented by this at higher photon energies. The claim of a 34.5 µm active layer was based on the assumption of the active region of the substrate having the same quantum efficiency as the epilayer. The thickness of the active layer may be different if the quantum efficiency of the substrate deviates significantly from that of the epilayer as a result of charge trapping or other loss mechanisms in the substrate.

The apparent contribution to the measured *FWHM* from incomplete charge collection noise was calculated by fitting the data at energies ≥ 5.41 keV (Cr $K\alpha_1$) and assuming a form aE^b (as per Eq. (4)). It was found that a = 0.03 and b = 1, with the electronic noise (A in Eq. (4))= 1650 eV ± 15 eV. The incomplete charge collection noise of the detector at Cr Ka_1 (5.41 keV) was found to be 162 eV. At the highest investigated energy (Pd Ka_1 = 21.17 keV) the incomplete charge collection noise was 635 eV. These apparent noise contributions were larger than the Fano noise at each energy (e.g. 153 eV at 5.41 keV; 303 eV at 21.17 keV) but much smaller than the electronic noise.

The energy resolutions achieved were modest compared with the highest quality custom SiC X-ray photodiodes ($FWHM$ = 196 eV at 5.9 keV [14]) and high quality GaAs X-ray photodiodes ($FWHM$ = 625 eV at 5.9 keV [41]; and $FWHM$ = 380 eV at 5.9 keV [2]). However, they were comparable to some custom SiC X-ray detectors ($FWHM$ = 1.6 keV at 5.9 keV [42] and $FWHM$ = 1.36 keV to 1.68 keV at 17.4 keV [43]) and better than has been achieved using other SiC UV photodiodes repurposed as X-ray detectors ($FWHM$ = 3 keV at 5.9 keV [44]).

3.3. Energy response linearity

In addition to other characteristics, such as energy resolution and quantum efficiency, an important characteristic of detectors for X-ray spectrometers for photon counting spectroscopy is their energy response linearity; this is the degree to which the charge output by the detector is linearly proportional to the energy of the incident photon. It has been previously shown that high energy linearity is achievable with compound semiconductor detectors [45]. Good understanding of the detector's performance in this regard is essential in order to achieve accurate calibration of the energy scale of X-ray spectra obtained with the device. The energy response linearity of an X-ray photodiode is influenced by factors including polarisation effects, charge trapping, and

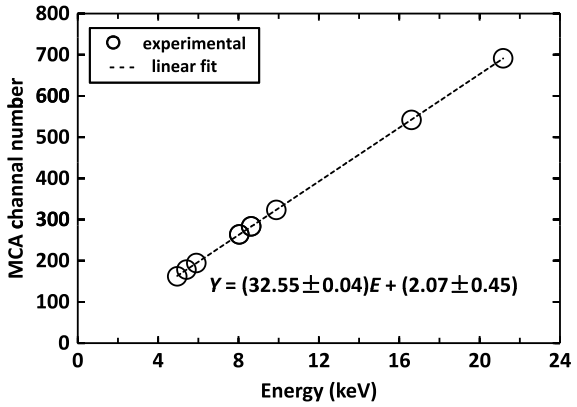

Fig. 6. The energy response linearity of the 0.06 mm^2 photodiode over the range 5 keV–21 keV. To determine the relationship between the incident photon energy, E (in keV), and the MCA channel number, Y, the positions of the centroids of the primary X-ray emission lines of the obtained spectra (in term of MCA channel number) were plotted as a function of the accepted energies of these emissions. The linearity error (evaluated by residuals of the fit in percentage terms) was found to be less than ± 0.7%.

charge collection efficiency [46]. In order to characterise the energy linearity of the SiC detector X-ray spectrometer, the spectra obtained of the eight high-purity fluorescence foils were fitted with Gaussians in order to determine in each case the multi-channel analyser (MCA) channel number at which the centroid of the primary X-ray fluorescence peak (see Table 1) was located. The positions of the photopeak centroids in terms of MCA channel number were then plotted as a function of photopeak energy in order to produce Fig. 6. In cases of multiple overlapping peaks (e.g. for the $K\alpha$ and $K\beta$ peaks of Ge, as shown in Fig. 5) the primary emission line peak was deconvolved from the detected combined photopeak to enable the position and energy of the primary photopeak to be used.

Linear least squares fitting showed that the relationship between the incident photon energy, E (in keV), and the MCA channel number, Y, was represented by the equation,

$$Y = (32.55 \pm 0.04)E + (2.07 \pm 0.45). \quad (5)$$

The fitting error bars (± 0.61 channels) associated with each data point were determined using the gradient and the y-axis intercept of the linear least squares fitting, which can be expressed as

$$S = \sqrt{\left(\frac{\sum \left(Y_i - \left(\left(\frac{n\sum(E_i Y_i) - \sum E_i \sum Y_i}{n\sum E_i^2 - (\sum E_i)^2} \right) E_i + \frac{\sum E_i^2 \sum Y_i - \sum E_i \sum (E_i Y_i)}{n\sum E_i^2 - (\sum E_i)^2} \right)^2 \right)}{n-2} \right)} \quad (6)$$

where, n is the number of data points, E_i is the photon energy, and Y_i is the MCA channel number, of the ith data point. This error bar was smaller than the analytical uncertainty associated with the determination of the centroid for each peak, and thus the data in Fig. 6 were appropriately fitted by a linear equation. The results show that despite the possible presence of some incomplete charge collection from photons absorbed in the device's substrate, the spectrometer's energy scale is still linear over the investigated range.

3.4. X-ray intensity measurements

Even the brightest cosmic X-ray sources provide relatively low X-ray fluences at the Earth's orbit (e.g. 150 photons cm^{-2} s^{-1} for Sco X-1 [47]). Consequently, detectors for such applications have to be high efficiency and are commonly accompanied by X-ray optics to improve detected count rates. However, the Sun is a significantly brighter X-ray source, and there is opportunity to make interesting X-ray heliophysics observations using simple and compact X-ray instrumentation carried on board CubeSats which do not benefit from X-ray optics [48]. X-ray observations of solar flares are one such area of interest, not least due to the significant impact solar flares can have on the geospace environment, including disrupting communications and navigation technologies, and damaging space hardware. As instrumentation which would be exposed to solar flares, the use of SiC rather than Si detectors in solar flare monitoring spacecraft is of interest due to the improved radiation-hardness of SiC. Solar flares can give rise to typical X-ray fluences at the Earth's orbit of ~ 10^5 to 10^6 photons s^{-1} cm^{-2} keV^{-1} at X-ray photon energies $\lesssim$ 10 keV [49], and reduced, but still significant, fluences at harder energies. For a 0.06 mm^2 detector as characterised in this article, this suggests detector incident fluences ~ 60 to 600 photons s^{-1} keV^{-1} at energies $\lesssim$ 10 keV.

In order to investigate the detector's response to illumination with different intensities (fluences) of X-rays, the count rate of the detector was investigated by fluorescing the Ge ($K\alpha$ = 9.88 keV and $K\beta$ = 10.98 keV) foil sample at five different X-ray tube currents from 0.2 mA to 1.0 mA, in 0.2 mA steps. The potential difference of the X-ray tube was kept at 35 kV throughout the measurements. To extend the range of fluences investigated, the experiment was conducted using two custom aluminium-PTFE X-ray collimators of different internal open diameters (8 mm ± 0.02 mm and 20 mm ± 0.02 mm) at each X-ray tube current, in turn. The collimators were designed such that all X-ray fluorescence from the aluminium cladding of the collimators was absorbed by the PTFE inners. The live time limit for accumulation of each spectrum was 6 h. The equipment was otherwise configured as per Section 3.2. The results of X-ray intensity measurements are shown in Fig. 7. To verify that the X-ray tube's emission fluence was linearly proportional to the X-ray tube's current, the X-ray tube's emissions were measured at each investigated tube current with a reference Si detector (LD Didactic 559 938) prior to the measurements of the Ge X-ray fluorescence with the SiC detector. The measurements with the Si reference detector confirmed the X-ray tube's linear proportionality.

A linear relationship was found between X-ray tube current and the SiC photodiode's detected count rate, ρ, (as defined by the number of counts contained within the Gaussian fitted to the deconvolved Ge $K\alpha$ peak for each tube current and collimator combination, divided by the spectrum's live limit accumulation time i.e. 6 h). By linear least squares fitting, the relationships were found to be described by the equations,

$$\rho_{8\ \mathrm{mm}} = (6.50 \pm 0.09)\, I + (0.09 \pm 0.06) \quad (7)$$

and

$$\rho_{20\ \mathrm{mm}} = (31.98 \pm 0.37)\, I - (0.07 \pm 0.25), \quad (8)$$

where $\rho_{8\ \mathrm{mm}}$ and $\rho_{20\ \mathrm{mm}}$ are the number of counts per second that contributed to the detected Ge $K\alpha$ peak when the 8 mm and 20 mm collimators were used respectively, and I is the X-ray tube current in mA. The error bars associated with each data point as determined by Eq. (6) were ± 0.06 counts s^{-1} and ± 0.24 counts s^{-1}, respectively. This is smaller than the analytical uncertainty associated with the determination of the number of counts in each fitted Gaussian and thus confirmed the appropriateness of a linear fit and hence that the response of the SiC spectrometer was linear at detected count rates from 1.4 counts s^{-1} to 31.7 counts s^{-1} at 9.88 keV. If the quantum efficiency of the detector at this energy was 0.02 (i.e. assuming a 2.69 μm active layer), these detected count rates correspond to incident 9.88 keV photon fluences of 70 photons s^{-1} to 1585 photons s^{-1} on the detector. If the quantum efficiency of the detector was 0.23 (i.e. assuming a 34.5 μm active layer) the count rates correspond to incident 9.88 keV photon fluences of 6 photons s^{-1} to 138 photons s^{-1} on the detector. Whilst it should be noted that solar flare X-ray spectra are not monochromatic, and thus the total energy deposited per second in a detector of this type when monitoring a flare will be greater than that investigated here, the results do provide an initial indication of the detector's potential suitability for this application in terms of count rate linearity near 10 keV.

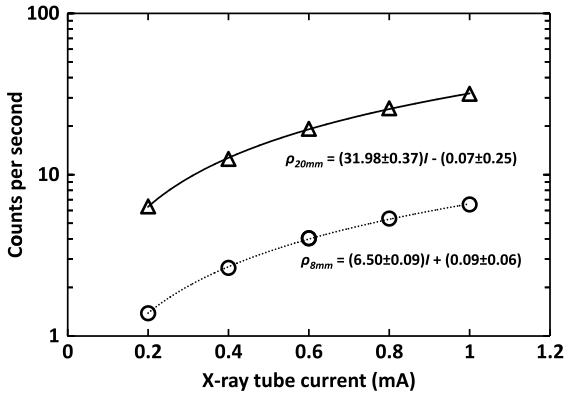

Fig. 7. X-ray intensity response of the SiC photodiode, showing the number of detected counts per second (defined as the number of counts contained within the Gaussian fitted to the Ge $K\alpha$ X-ray fluorescence peak divided by the spectrum accumulation time) as a function of X-ray tube current. Count rates are shown when using collimators with 8 mm (open circles) and 20 mm (open triangles) diameter apertures. The linearity error (evaluated by residuals of the fit in percentage terms) was less than ± 2%.

4. Conclusions and future work

A 0.06 mm^2 commercial 4H-SiC UV p-n photodiode has been investigated for its performance as a detector for photon counting X-ray spectroscopy at photon energies from 4.95 keV to 21.17 keV. The X-ray performance of the detector when connected to a custom-made low-noise charge-sensitive preamplifier was investigated by illuminating the detector with fluorescence X-rays (of energy 4.95 keV–21.17 keV) from 8 different high purity metal foils which were fluoresced by a Mo cathode X-ray tube operated at 35 kV and 1 mA. The detector and preamplifier were operated uncooled at a temperature of 33 °C.

The results showed that the spectrometer had an energy resolution (*FWHM*) of 1.6 keV–1.8 keV across the energy range when operated at + 33 °C. The charge detected (and hence the spectrometer's output) was found to be a linear function of the photon energy, despite some possible incomplete charge collection noise from photons absorbed in the substrate of the detector. The number of counts per second detected by the spectrometer was also found to be linearly dependent on the incident X-ray fluence over the count rate range investigated. Although the energy resolutions achieved with this detector were not as good as some custom X-ray detectors [14], its low cost and wide commercial availability, together with its ability to operate uncooled, and the visible blindness and radiation hardness of SiC, make it an interesting and potentially useful detector for numerous applications, including solar flare monitoring on board CubeSats.

Acknowledgements

This work was in part supported by the Science and Technologies Facilities Council, UK, through grant ST/M004635/1 (University of Sussex, A.M.B., PI). A.M.B. acknowledges funding received from The Leverhulme Trust, UK, in the form of a 2016 Philip Leverhulme Prize.

Authors' Data Statement: Data underlying this work are subject to commercial confidentiality. The Authors regret that they cannot grant public requests for further access to any data produced during the study.

References

[1] D.S. McGregor, H. Harmon, Nucl. Instrum. Methods A 395 (1997) 101.
[2] A. Owens, et al., Nucl. Instrum. Methods A 479 (2002) 531.
[3] G. Lioliou, X. Meng, J.S. Ng, A.M. Barnett, J. Appl. Phys. 119 (2016) 124507.
[4] J. Lauter, D. Protić, A. Förster, H. Lüth, Nucl. Instrum. Methods A 356 (1995) 324.
[5] M.D.C. Whitaker, G. Lioliou, S. Butera, A.M. Barnett, Nucl. Instrum. Methods A 840 (2016) 168.
[6] A.M. Barnett, G. Lioliou, J.S. Ng, Nucl. Instrum. Methods A 774 (2015) 29.
[7] S. Butera, et al., J. Appl. Phys. 120 (2016) 174503.
[8] A. Auckloo, et al., J. Instrum. 11 (2016) P03021.
[9] L. Abbene, et al., Nucl. Instrum. Methods A 835 (2016) 1.
[10] Y. Eisen, A. Shor, J. Cryst. Growth 184/185 (1998) 1302.
[11] G. Bertuccio, R. Casiraghi, F. Nava, IEEE Trans. Nucl. Sci. 48 (2001) 232.
[12] G. Bertuccio, R. Casiraghi, IEEE Trans. Nucl. Sci. 50 (2003) 175.
[13] F. Nava, G. Bertuccio, A. Cavallini, E. Vittone, Meas. Sci. Technol. 19 (2008) 102001.
[14] G. Bertuccio, S. Caccia, D. Puglisi, D. Macera, Nucl. Instrum. Methods A 652 (2011) 193.
[15] K.C. Mandal, P.G. Muzykov, J.R. Terry, Appl. Phys. Lett. 101 (2012) 051111.
[16] K.C. Mandal, P.G. Muzykov, S.K. Chaudhuri, J.R. Terry, IEEE Trans. Nucl. Sci. 60 (2013) 2888.
[17] G. Bertuccio, D. Puglisi, A. Pullia, C. Lanzieri, IEEE Trans. Nucl. Sci. 60 (2013) 1436.
[18] A. Torrisi, et al., IEEE Trans. Electron Devices 64 (3) (2017) 1120.
[19] G. Bertuccio, Nucl. Instrum. Methods. Phys. Res. A 546 (2005) 232.
[20] G. Bertuccio, et al., IEEE Trans. Nucl. Sci. 53 (4) (2006) 2421.
[21] S. Seshadri, et al., IEEE Trans. Electron Devices 46 (1999) 567.
[22] G. Bertuccio, et al., Appl. Surf. Sci. 272 (2013) 128.
[23] A. Lo Giudice, et al., Mater. Sci. Forum 483 (2005) 389.
[24] G. Bertuccio, Micro- and Nanotechnology Sensors, Systems, and Applications II, in: Proc. SPIE, vol. 7679, 2010, p. 76790T.
[25] G.W. Fraser, Extraterrestrial analysis: Planetary X-ray fluorescence from orbitig spacecraft and landers, in: Portable X-ray Fluorescence Spectrometry: Capabilities for in Situ Analysis, RSC Pub., Cambridge, 2008.
[26] F.D. Seward, P.A. Charles, Exploring the X-ray Universe, Cambridge University Press, 2010.
[27] L. Duvet, et al., High Energy, Optical, and Infrared Detectors for Astronomy VI, in: Proc. SPIE, vol. 9154, 2014, p. 915403.
[28] Anon, Broadband SiC based UV photodiode A = 006 mm^2, SG01S–18, Rev. 60, SGlux SolGel Technologies GmbH, Berlin, Germany, N.D.
[29] S. Zhao, T. Gohil, G. Lioliou, A.M. Barnett, Nucl. Instrum. Methods A 830 (2016) 1.
[30] S. Zhao, G. Lioliou, A.M. Barnett, Nucl. Instrum. Methods A 859 (2017) 76.
[31] D. Prasai, et al., J. Mater. Res. 28 (1) (2013) 33.
[32] S.M. Sze, Physics of Semiconductor Devices, third ed., John Wiley & Sons, New Jersey, 2007.
[33] L. Patrick, W.J. Choyke, Phys. Rev. B 2 (1970) 2255.
[34] G.W. Fraser, X-ray Detectors in Astronomy, Cambridge University Press, Cambridge, 1989.
[35] A.M. Barnett, J.E. Lees, D.J. Bassford, J. Instrum. 8 (2013) P09014.
[36] G. Bertuccio, A. Pullia, G. De Geronimo, Nucl. Instrum. Methods A 380 (1996) 301.
[37] A.M. Barnett, J.E. Lees, D.J. Bassford, J.S. Ng, Nucl. Instrum. Methods A 673 (2012) 10.
[38] M. Sánchez, et al., XRAYLIB Tables (X-ray Fluorescence Cross-Section), European Synchrotron Radiation Facility and University of Sassari, 2003.
[39] A. Owens, Compound Semiconductor Radiation Detectors, CRC Press, Boca Raton, 2012.
[40] A. Owens, et. al, J. Appl. Phys. 90 (2001) 5376.
[41] G. Lioliou, A.M. Barnett, Nucl. Instrum. Methods A 836 (2016) 37.
[42] A.M. Barnett, (Ph.D thesis), 2011, University of Leicester.
[43] G. Lioliou, et al., Nucl. Instrum. Methods A 840 (2016) 145.
[44] J.E. Lees, A.M. Barnett, D.J. Bassford, M. Mazzillo, J. Instrum. 7 (2012) P11024.
[45] G. Bertuccio, et al., IEEE Trans. Nucl. Sci. 44 (1997) 1.
[46] G.F. Knoll, Radiation Detection and Measurement, John Wiley, Hoboken, NJ, 2010.
[47] J.V. Paradijs, J.A.M. Bleeker, X-ray Spectroscopy in Astrophysics, Springer-Verlag, Berlin Heidelberg, 1999.
[48] T.N. Woods, et al., Astrophys. J. 835 (2017) 122.
[49] A.O. Benz, et al., Space Telescopes and Instrumentation 2012: Ultraviolet to Gamma Ray, in: Proc. SPIE, vol. 8443, 2012, p. 84433L.